Interaction of small carbon molecules and zinc dichloride: DFT study

J.H. Pacheco-Sánchez[a,*], I.P. Zaragoza-Rivera[b] and A. Bravo-Ortega[c]
[a]*Division de Estudios de Posgrado e Investigación, Instituto Tecnológico de Toluca,*
Metepec, 52149, Edo. Mex., México,
Tel: 527222087224;
Av, Tecnológico S/N, Col. Agrícola Bellavista, Metepec 52149,
Estado de México, México,
Tel: 527222087200 ext. 3211;
e-mail: jpachecos@toluca.tecnm.mx
[b]*Division de Estudios de Posgrado e Investigación, Instituto Tecnológico de Tlalnepantla,*
Tlalnepantla, 54070, Edo. Mex., México,
Tel: 525553900310,
e-mail: ipzaragoza@exalumno.unam.mx
[c]*Instituto Tecnológico y de Estudios Superiores de Monterrey,*
Atizapán de Zaragoza, 52926, Campus Edo. Mex, México,
Tel: +525558645669;
e-mail: abravo@itesm.mx

Received 17 February 2016; accepted 4 November 2016

The interaction between carbon molecules and zinc dichloride molecules ($ZnCl_2$ - zinc salt) comes to be evident by means of small molecular systems of six-carbon (linear or rings) and zinc salt. The interaction is evident through the potential energy surface (PES) of the interacting system at the ground state, starting with a molecular geometry optimization of the energy in order to get equilibrium energy of potential energy surfaces PES. This is one way to start understanding of the porous form of an adsorbent material known as activated carbon. We recognize six-carbon fragments as amorphous activated carbon after geometry optimization with zinc dichloride, which appear in several planar and non-planar forms. An adsorbent material of pollution known as activated carbon can be obtained when carbon molecules are exposed to zinc salt ($ZnCl_2$) molecules. Some cases of the morphology of these systems are accomplished at the density functional theory level (DFT) using GGA-PW91 for exchange and correlation with dnd basis functions.

Keywords: Potential energy surface; molecular systems; geometry optimization; density functional theory.

La interacción entre moléculas de carbón y moléculas de dicloruro de zinc ($ZnCl_2$) se hace evidente por medio de sistemas moleculares de pequeñas moléculas de seis-carbones (lineales o anillos) y sal de zinc. La interacción es evidente a través de superficies de energía potencial (PES) del sistema interactuante en el estado base, empezando con una optimización de geometría molecular de la energía para obtener la energía de equilibrio de la superficie de energía potencial PES. Esta es una manera de empezar a entender la forma porosa de un material adsorbente conocido como carbón activado. Reconocemos fragmentos de seis-carbones como carbón activado amorfo con sal de zinc, que aparecen en varias formas planas y no-planas. Un material adsorbente de contaminantes se puede obtener cuando las moléculas de carbón se exponen a moléculas de sal de zinc ($ZnCl_2$). Algunos casos de la morfología de estos sistemas se logran con un nivel de teoría de funcionales de la densidad (DFT) usando GGA-PW91 para intercambio y correlación con funciones base dnd

Descriptores: Superficies de energía potencial; sistemas moleculares; optimización de geometría; teoría funcional de la densidad.

PACS: 34.20.Gj

1. Introduction

The study of the interaction energy among systems of six-carbon molecules and one zinc-dichloride molecule provides a potential energy curve indicative of the nature of the adsorbent material. Potential energy curves in two dimensions arise from the projection of potential energy surfaces in one plane. We consider that after the interaction, the carbon fragments obtained correspond to amorphous activated carbon (AC) either in planar or non-planar geometry. Planar corresponds to graphitizing AC, while adsorbent material represented by means of several surfaces fragments considered as hydrogen adsorbents.

Activated carbon use to be synthesized at different pore shape distributions by diverse methods at different temperatures and pressures [1]. Measurements of BET surface areas, SBET, give 1740 m^2 g^{-1} for activated carbon powder (ACP) and 1970 m^2 g^{-1} activated carbon fiber (ACF) [2]. The SBET of the ACF was 1.13 times larger than that of the ACP calculated.

In a previous research [3] of burned coconut shells, the carbon obtained was activated using zinc dichloride [$ZnCl_2$]. BET surface area measurements provided 208, 342, 452, 452 [m^2/g] at 600, 700, 800, 900 [°C] respectively. The corresponding pore size diameters were 15, 14.8, 14.5, 14.5 [Å] obtained. Activated carbon with $ZnCl_2$ as activating agent

also was found to have pore size diameter: 17.6-18.4 Å [4]. According to the micropore size distributions (MPSD) measurements of activated carbon [5], the most populated results are around 9 Å at the interval 6 to 18 angstroms, on which two different types of carbon materials were prepared: (i) chemically activated carbons prepared from an anthracite and a bituminous coal using KOH as activating agent, and (ii) physically activated carbon fibers prepared from petroleum pitch and coal tar pitch-based carbon fibers, by activation with CO_2 and steam. Finally, the pore size distribution of activated carbons from adsorption data of different adsorbates was estimated by several methods [6]; particularly in the adsorption of nitrogen the range is 6-10 Å where their Eq. (9) lead them to the highest values of the average micropore width, while their Eqs. (13) and (14) lead them to the lowest ones.

Activated carbon is broadly defined to include a wide range of amorphous carbon based materials prepared in such a way that they exhibit high degree of porosity and an extended surface area [7]. Some researchers consider that the structure of activated carbon is quite similar to that of graphite composed of microcrystallites consisting of fused hexagonal rings of carbon atoms [8]. The spaces between the individual microcrystallites are called pores. Most of the adsorption takes place in micropores. Amorphous activated carbon is manufactured in many different forms: granular, fiber, and powder, as a few number of them.

The precise atomic structure of activated carbon is unknown [9]. The first carbon structures were found by means of pyrolysis, these carbons fall into two distinct classes: graphitizing and non-graphitizing. Choosing a particular activated carbon (carbonized from peat in an inert atmosphere at 500°C) and through HRTEM micrographs, growth of curved and faceted carbon sheets as blankets of (pentagonal, hexagonal and heptagonal) carbon rings networks displaying curvature can be observed, in some cases as bags enclosing much larger pores than in the fresh carbon [10].

Diffusion of alkali ions on amorphous carbon by means of ab initio molecular dynamics for elucidating the interaction nature between K^+/K and amorphous carbon was studied [11] using seven different graphene sheets of hexagonal carbon rings, and considering them as models of amorphous carbon. A reaction mechanism of CF_3I synthesis catalyzed by activated carbon was investigated with quantum chemistry methods using DFT [12], obtaining: i) the adsorption configuration of some intermediates considering dehydrofluorination of CHF_3 catalyzed by -COOH groups, which possess the highest barrier (ii) the difluorocarbene disproportionation over graphite (001) surface, and (iii) the corresponding pathway through TS_{1-2}.

Random vs. realistic amorphous carbon models were confronted [13] using measurements of high resolution microscopy and electron diffraction. The approach is to simulate a realistic carbon from an energetic model based on the tight-binding approximation. Then, a comparison of this carbon with the carbon obtained by randomly generated carbon atom positions, and concluding that the limit thickness for the weak phase approximation is 30% overestimated.

In the case of chemical activation several substances have been employed; however, the $ZnCl_2$ has received special attention due to a high dehydrator effect that is conferred to raw material which attacks in solution to not extreme temperatures, promoting a fast and effective degradation of the cellulose material that makes up the majority of nuts and coconut shells [14-16], coffee [17], wood sawdust [18,19], olive and prune seeds, walnut nut shells, paper, and organic materials [20].

Active carbons are mainly and almost exclusively prepared by pyrolysis of carbonaceous raw material at temperatures lower than 1000°C. Activated carbon formed under the action of $ZnCl_2$ is an adsorbent material proposed to study properties of hydrogen adsorption, and exhibits structural modification where the carbon is by means of $ZnCl_2$ molecular arrangement activated. Structural properties might be for hydrogen adsorption-desorption processes considered.

Knowing that carbonization generates dehydrogenated carbon we consider hypothetical carbon molecules having zero content of hydrogen. And also knowing that carbon is the major constituent of active carbons [7], and is present to the extent of 85% to 95%, in this work hypothetical molecules of either six-carbon chains or polyyne HC_6H or hexagonal carbon rings are confronted to one $ZnCl_2$ molecule. Some mechanisms of the reaction involved in the activation of carbon chains and diamond-like carbon by $ZnCl_2$ are also considered. The calculations of energy by means of exchange and correlation functional using dnd basis sets of functions were accomplished.

2. Modeling and computational methodology

In order to figure out about suitable arrangements, we achieved DFT calculations of geometry optimization on molecular systems $[C_6]_nZnCl_2$ or $[HC_6H]_nZnCl_2$ arising from the reaction of either n-hypothetical six-carbon (chains or rings) or n-polyyne with a $ZnCl_2$ molecule respectively. A geometry optimization gives the dissociation energy of the interacting molecules. In order to know the size of the potential well, single point calculations in order to obtain potential energy curves are achieved.

This arrangement is in symmetry group C_1 investigated, through DFT electronic structure program [21], using PW91 exchange-correlation functional in the generalized gradient approximation (GGA) [22,23]. The calculations are all-electron and spin-unrestricted (different orbital for different spin). Open-shell systems are accomplished with unrestricted wave functions. For these molecules, we use a dnd double numerical basis with polarization functions, *i.e.*, functions whose angular momentum is higher than that of the highest occupied molecular orbital in the free atom. The size of the dnd basis is comparable to 6-31G** basis sets. Diamond-like carbons are investigated through DFT-m-GGA-M06-L functional, dnd basis, DIIS, and smearing of 0.9 Ha.

Connectivity [24] calculations according to DMol^3 on no bonding to s- and f-shell scheme, bond type, and converting representation to Kekulé, for bond length tolerances from 0.6 to 1.15 Å were accomplished in some cases of graphitic carbon.

Area calculations have been carried out by inserting triangles in each amorphous carbon ring and using the Heron formula: $A = \sqrt{(P(P-a)(P-b)(P-c))}$, where $P = (a+b+c)/2$ is the perimeter of a triangle of a, b, c sides; while the pore size diameter (PSD) is calculated as an approximation to the circle area.

3. Results

First of all, calculations in order to get credibility for using DFT in small systems are accomplished. Then, either polyyne or linear carbon, hypothetical six-carbon, and hexagonal carbon rings without hydrogen are confronted to zinc dichloride in order to obtain equilibrium energies. In spite of we are considering carbon molecules as hypothetical, we mention the kind of hybridization they correspond. All the results are in the following sections obtained.

3.1. Carbon-carbon interaction

In order to get a better idea of the order of magnitude of the approach of this methodology, carbon-carbon interaction has been calculated. A geometry optimization provides the minimum (1.3Å, -161.863 kcal/mol), which corresponds to the equilibrium point. The whole reaction pathway is shown in Fig. 1; where 156.3 kcal/mol as dissociation energy is obtained. While in the ground state $D_0^0 = 6.21$ eV = 143.22 kcal/mol corresponds to experimental measurement [25]. Then, the difference is 9.13%, corresponding to an overestimated energy lower than 10%.

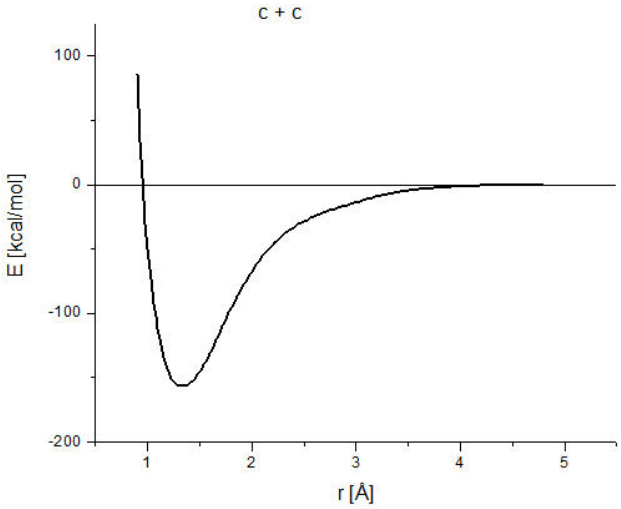

FIGURE 1. Here we observe the pathway of reaction or the potential energy curve of the carbon-carbon interaction. The bond strength is 156.3 kcal/mol.

Zinc and chlorine interaction energy with the same methodology was also calculated. The resulting dissociation energy of the ground state 50.53 kcal/mol agrees in 4.3% of difference with experimental [25] value $D_0^0 = 2.1$ eV = 48.43 kcal/mol.

In addition the geometry optimization of Cl - Cl interaction was carried out. These create the molecule Cl_2 at 2.023 Å of separation and the resulting dissociation energy of the ground state 56.802 kcal/mol agrees with the experimental value $D_0^0 = 2.47936$ eV = 57.181 kcal/mol [25]. Then a zinc atom with a separation 2.693 Å of every chlorine atom was added for calculating geometry optimization again. A binding energy -159.78 kcal/mol was after 23 steps obtained. Then, zinc atom stayed inserted in the middle of the two Chlorine atoms forming the $ZnCl_2$ linear molecule with bonds of 2.104 Å and 180° ClZnCl angle.

3.2. Hypothetical (-C≡C-)$_3$ plus $ZnCl_2$ interaction

Sequences of input-output molecular arrangements are shown in Fig. 2. Table I exhibits the equilibrium energies of the corresponding geometry optimization of this system and the bond strength. The first three parts (a, b and c) of Fig. 2 correspond to one hypothetical six-carbon chain alternating single and triple bonds (-C≡C-)$_3$ and interacting with one zinc salt molecule in sp molecular hybridization. The only one difference in the input in each case is the initial separation among the reactants: a) 0.702 Å, b) 1.221 Å and c) 2.000 Å. The output exhibit strong differences: a) one bond of zinc salt decreased from 2.127 Å to 2.106 Å and the other increased until 5.312 Å; the reactants started linear and ended bent by 143° of the carbon chain molecule, and 129.048° of the zinc salt molecule. b) The zinc salt ended occupying the hydrogen places forming a whole linear chain molecule. c) The separation among the reactants increased from 2 Å to 3.85 Å indicating repulsion, and the linearity 180° changed to 177.4° for carbon chain and 174.105° for zinc salt.

The last three parts (d, e, and f) in Fig. 2 correspond to two hypothetical six-carbon chains 2(-C≡C-)$_3$ interacting with one zinc salt molecule where the distance among the reactants is shown in the input of Fig. 2. The output exhibits strong differences: d) the ClZnCl angle changed from 180° to 172.393°, the repulsion is from 1.1 Å until 4.166 Å, and

TABLE I. Equilibrium distance and energy along with the energy at infinity allow the calculation of the bond strength as $E_{\text{bond strenght}} = |E_\infty - E_e|$. Energy in [Kcal/mol], distance in [Å].

Input	R_e	E_e	E_∞	Bond strength
a	2.664	-1007.446	-853.423	154.02
b	0	-1062.913	-861.146	201.80
c	3.85	-963.592	-963.075	0.52
d	2.664	-1901.792	-1899.331	2.46
e	0	-1913.909	-	
f	4.057	-1905.538	-1903.604	1.93

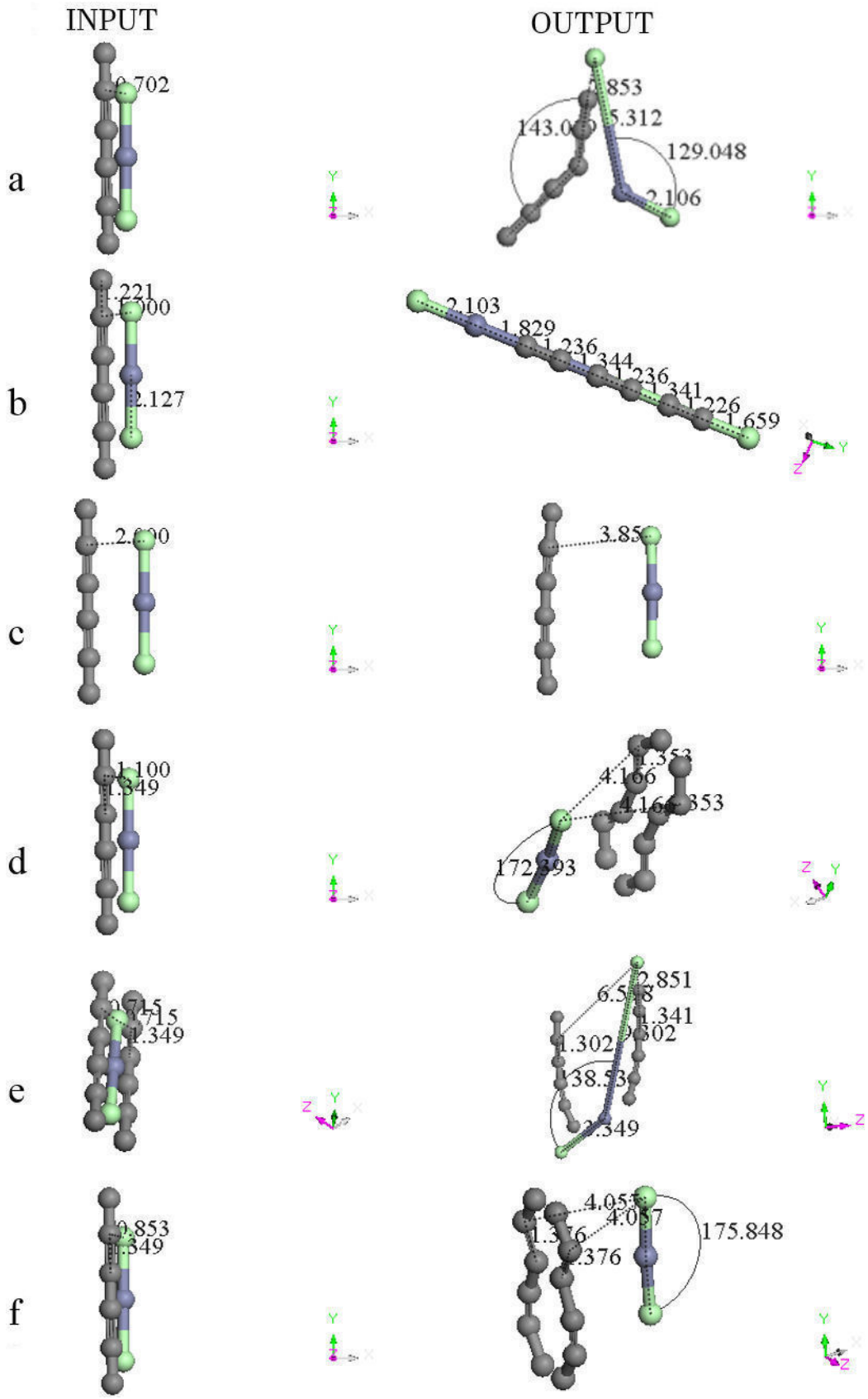

FIGURE 2. A sequence of input - output molecular arrangements are shown. a) b) and c) correspond to one six-carbon chain interacting with one zinc salt molecule. And d) e) and f) correspond to two six-carbon chain interacting with one zinc salt molecule.

carbon planar molecule tend to form six-ring. e) the ClZnCl angle changed from 180° to 138.530°, the repulsion allows the whole system 2(-C≡C-)$_3$ZnCl$_2$ as a planar molecule. f) the ClZnCl angle changed from 180° to 175.848°, the repulsion is from 0.853 Å to 4.057 Å, and carbon planar molecule tend to form one six-ring and one eight-ring.

3.3. 2C$_6$ hypothetical chains plus Zn interaction

The molecular hybridization is mixed sp^2 and sp^3 for carbons in the body and at the end of the chain, respectively. Considering the molecular arrangement of one metal atom (Zn) between two parallel linear hypothetical six-carbon chains 1.54 Å separated as shown in Fig. 3a, a binding energy -1688.930 kcal/mol outcome from this geometry optimization of 64 steps with a Zn atom near to two crossed carbon chains as in Fig. 3b, where the whole system corresponds to a non-planar geometry arrangement. This result indicates that carbons arrangement corresponds to amorphous carbon.

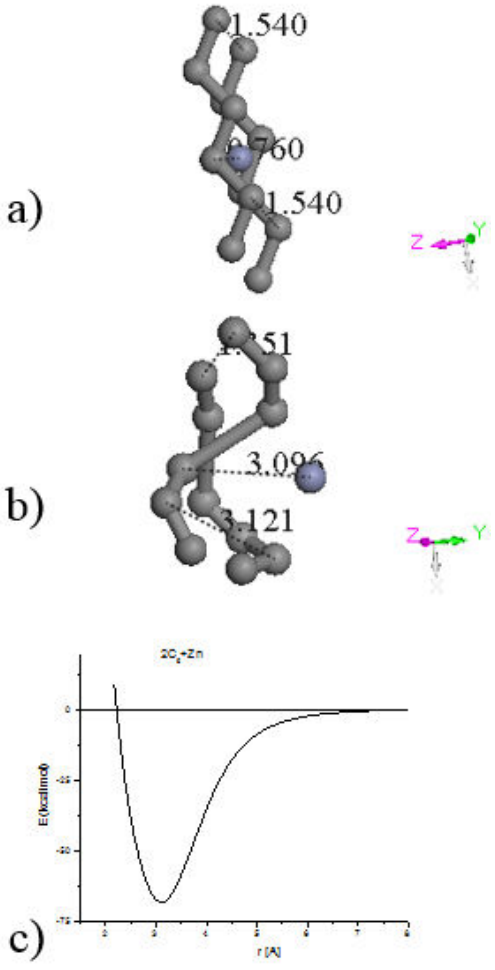

FIGURE 3. a) Input: Zinc atom between two linear hypothetical six-carbon chains. b) Output: a non-planar C$_6$ZnC$_6$ optimized structure. It is clear an amorphous tendency of carbons arrangement in this geometry optimization. c) Potential energy curve calculation of single point where the minimum corresponds to the dissociation energy of (2C$_6$)Zn molecule.

TABLE II. Well depth size for a potential energy curve. Energy in [Kcal/mol] and distance in [Å].

Molecular interaction	Energy	Distance
2C$_6$+Zn	70	3.1
2C$_6$+ZnCl$_2$	175	1.9

A potential energy curve between two six-carbon-chains and one Zn atom was determined. Calculations at 1-7 Å distances between one carbon atom in the molecule and one zinc atom as observed in Fig. 3c were achieved, by using small distance increments step by step with the purpose of determining the possible existence of adsorption. Adsorption due to the depth 68 kcal/mol of the potential well was found.

The interaction of two six-carbon chains with zinc atom is studied. First, the interaction energy values present a repulsive effect among these molecules at different separation distances: 2-3.1 Å. Second, they present an attractive effect from 3.1 to ∼7 Å of separation distances indicating that there is an adsorption of the Zn atom on two six-carbon chains. Then, the 2C$_6$Zn molecule is formed at the minimum (-68 kcal/mol, 3.1 Å) of the pathway (see Fig. 3c, Table II).

In addition since zinc is an acid (acceptor) [26] receiving an electron pair in its lowest unoccupied molecular orbital (LUMO) from the highest occupied molecular orbital (HOMO) of a base (donor). That is, the HOMO from the base and the LUMO from the acid combine with a bonding molecular orbital, which in our case corresponds with the orbital 102-HOMO and 103-LUMO, for Fermi Energy -5.107 eV, in the A irreducible representation of the C$_1$ symmetry. The total number of valence orbitals is 192. The orbital occupation is 49 A (1) alpha and 49 A (1) beta, and 2.00 alpha electrons in 4 orbitals plus 2.00 beta electrons in 4 orbitals, for a total 102.0 number of electrons; and a binding energy -1688.930 kcal/mol.

3.4. 2C$_6$ hypothetical chains plus ZnCl$_2$ interaction

The hypothetical carbon chains have mixed sp^2 and sp^3 molecular hybridization. The molecular arrangement of one ClZnCl linear molecule between two parallel linear hypothetical six-carbon chains 1.54 Å separated as shown in Fig. 4a is for starting a geometry optimization considered. A binding energy -1891.068 kcal/mol result from this geometry optimization of 105 steps with a ZnCl$_2$ non-linear molecule near to two crossed carbon chains, where the whole system corresponds to a non-planar geometry arrangement as seen in Fig. 4b. Another orientation of this Figure exhibits 1.36 Å instead of the initial 1.54 Å in one extremity, a bonding crossing in the other with a new bond 2.508 Å, and 1.735 [Å] of molecular separation (Fig. 4c). With this result it is clear that carbons arrangement is neither ring nor linear chain, certainly with porosity.

Initially, the interaction energy values present a repulsive effect among these molecules at different separation dis-

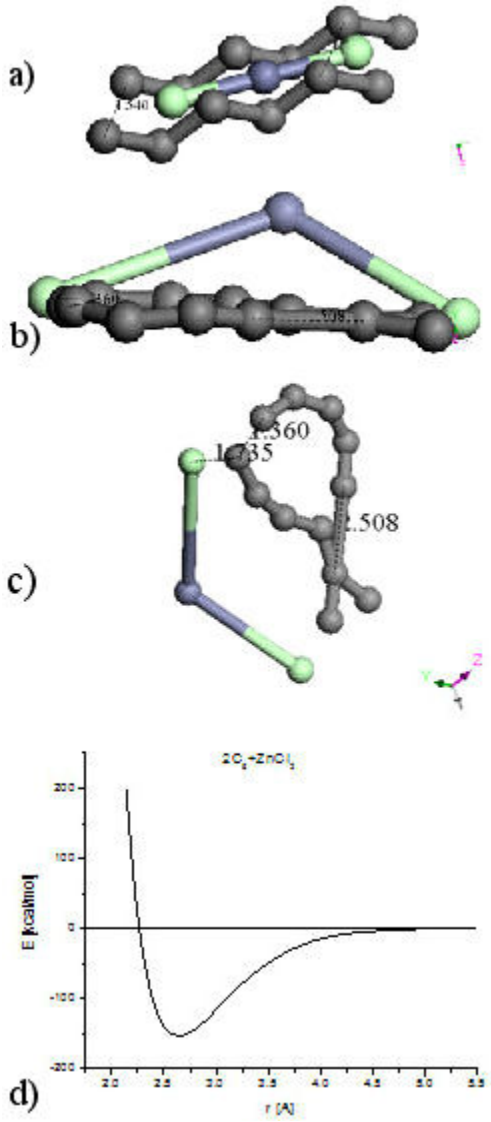

FIGURE 4. a) Input: Zinc atom into two chlorine atoms plus two 6-carbon linear chains. b) Output 1: a non-planar $(2C_6)ZnCl_2$ optimized structure, where $2C_6$ molecule is planar. c) Output 2: It is clear an amorphous tendency of carbons arrangement in these two geometry optimizations. d) The optimization energy calculation means an adsorption of amorphous activated carbon on Zinc salt at the minimum of the potential energy curve calculation of single point.

tances: 2-2.6 Å as in Fig. 4d. Next, the two six-carbon chains system and the molecule containing hydrogen present an attractive effect from 2.6 to ∼4.5 Å of separation distances indicating that there is an adsorption of the $ZnCl_2$ molecule on the two six-carbon chain. Then, the $[2C_6]ZnCl_2$ molecule is formed at the minimum (-153.5 kcal/mol, 2.64 Å) of the pathway (see Fig. 4d).

The linear $ZnCl_2$ molecule between two 6-linear chains (see Fig. 4a) was also optimized, obtaining $[2C_6]ZnCl_2$ as observed in Figs. 4b and 4c in different orientations.

The potential energy curve among two six-carbon-chains and a $ZnCl_2$ molecule as in Fig. 4d was determined. Calculations at 1-10 Å distances between these two molecules were achieved, as observed in Fig. 4c, by using small distance increments with the purpose of determining the possible existence of an adsorption. An adsorption due to the depth 150 kcal/mol of the potential well was found.

The HOMO from the base and the LUMO from the acid combine with a bonding molecular orbital, which in our case corresponds to the orbital 136-HOMO and 137-LUMO, for a Fermi Energy of -5.222 eV, in the A irreducible representations of the C_1 symmetry. The total number of valence orbitals is 228. The orbital occupation is 66 A (1) alpha and 66 A (1) beta, and 3.00 alpha electrons in 4 orbitals plus 3.00 beta electrons in 4 orbitals, for a total 138.0 number of electrons; and a binding energy of -1891.068 kcal/mol.

A small change on the position of the zinc salt linear molecule among the two carbon chains (Fig. 5a) was applied, and another geometry optimization shown in Fig. 5b was found, consequently the morphology of the activated carbon is different to the previous one; however, it is still amorphous. The relevant fact is that the potential well is 175 kcal/mol of depth (see Fig. 5c, Table II), which is greater than the previous one.

3.5. Polyyne carbon chains plus $ZnCl_2$ interaction

Previously, hypothetical single bond carbon chain dehydrated and dehydrogenated has been chosen in order to see its morphology. In this case the bond strength of carbon-chains with zinc (Fig. 3c) is around half of that for carbon-chains with zinc-salt (Fig. 5c). In this address, an example of a known hydrogenated linear carbon chain is polyyne carbon, which is an allotrope of carbon that has a chemical structure $H(\text{-}C{\equiv}C\text{-})_nH$ as a repeating chain, with alternating single and triple bonds [27] and hydrogen at every extremity as any member of the polyyne [28] family $HC_{2n}H$ corresponding to sp hybridization atoms.

A geometry optimization is applied on different arrangements of the zinc salt molecule interacting with $H(\text{-}C{\equiv}C\text{-})_3H$ polyyne molecules (See Fig. 6 and Table III). The output of Fig. 6 shows the geometry of the activated carbon, which we

TABLE III. Initial separation is in angstroms and ClZnCl angle is in degrees of the input-output optimization geometry shown in Fig. 6.

INPUT			OUTPUT	
Molecular arrangement	Initial separation	ClZnCl Angle	New Molecule	nHC_6H molecular structure
a	1.0[Å]	164.875°	$ZnCl_2[HC_6H]$	Linear
b	1.1[Å]	172.092°	$ZnCl_2[2HC_6H]$	Planar
c	3.723[Å]	174.802°	$ZnCl_2[3HC_6H]$	Planar
d	1.1[Å]	172.480°	$ZnCl_2[2HC_6H]$	Planar
e	1.23[Å]	150.309°	$ZnCl_2[2HC_6H]$	Non-planar
f	4.002[Å]	177.491°	$ZnCl_2[2HC_6H]$	Non-planar
g	1.006[Å]	171.249°	$ZnCl_2[3HC_6H]$	planar

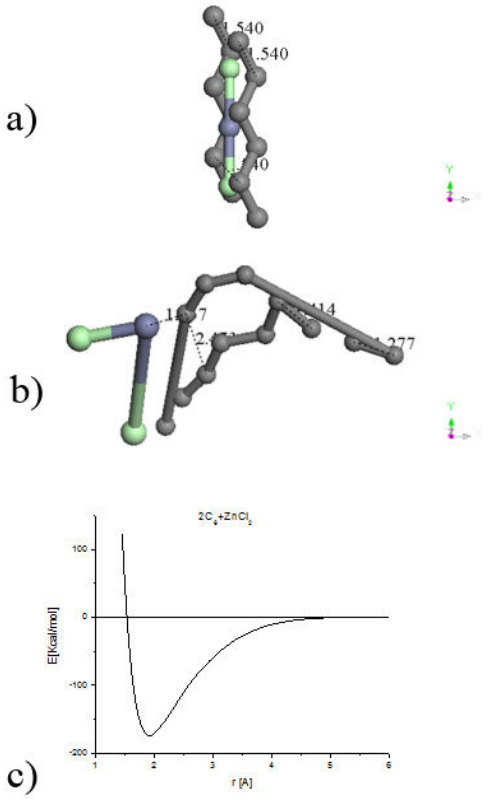

FIGURE 5. a) Input: Zinc atom into two chlorine atoms plus two 6-carbon linear chains at a small change of Fig. 4a, b) Output 1: a planar $(2C_6)ZnCl_2$ optimized structure. c) We observe the potential energy curve with 175 kcal/mol of well depth.

TABLE IV. Equilibrium distance R_e and equilibrium energy E_e corresponding to the minimum of each potential energy curve in Fig. 7. Energy in [Kcal/mol], and distance in [Å].

Input	R_e	E_e
a	3.4	-2.8
b	4.0	-2.75
c	4.1	-1.59
d	4.1	-2.05
e	2.8	-10.22
f	5.20	-2.21
g	4.1	-2.14

are to describe to continuation: a) A linear carbon chain, b) Flat carbon chain molecules separated 4.033 Å, c) Three curvilinear carbon chain separated at the extremities and forming a weird six carbon ring in the center, where the whole carbon system is located in one geometric plane, d) Two carbon chain molecules separated in one side and forming an eight carbon ring two bonds open in the other side, e) non-planar carbon chain molecules in an S geometric form, f) two parallel semi-cylindrical carbon chain molecules g) two carbon molecules with zinc salt form four six-carbon rings. The graphs of the potential energy curves of Fig. 6 are exhibited in Fig. 7, and the corresponding equilibrium energies are given in Table IV.

3.6. Hexagonal carbon rings plus $ZnCl_2$ interaction

We start calculating DFT geometry optimization of one hexagonal carbon ring with only one zinc metal atom in its center. The hybridization of ring carbons is sp^2. After the optimization, a 35.10% area growth or $A_O = 1.3510A_I$ for $A_I = 6.1616A_2$ (see Figs. 8a) was calculated, where A_I is the input area and A_O is the output area; while using one linear zinc salt ($ZnCl_2$) molecule perpendicularly to the plane of the ring produces 43.53% area growth or $A_O = 1.4353A_I$ as observed in Figs. 8b. The largest part of the growth comes from the metal atom, however zinc salt gives greater growth than zinc and can be removed from carbon by washing with water, while zinc stays adsorbed in carbon molecules. Table V provides binding energies, and pore size diameters in a whole output system PSDW and in the biggest ring PSDR for every output illustration in Fig. 8.

In the rest of this work we will use sheets of hexagonal carbon rings at interaction with linear zinc salt as input to the simulation, where zinc is located in the middle of the linear optimized zinc salt, in order to calculate geometry optimization of the whole system.

Adding one hexagonal carbon ring to the previous one as input (see Fig. 8c) for calculating the geometry optimization take us to the output in this case. It is very clear the amorphous form of the activated carbon in this result, in which the zinc salt passed through one bond of a carbon ring until a distance of 1.318 Å, and the equilibrium energy -1609.841 kcal/mol corresponds to chemisorption [29]. The initial form of these two rings was seriously distorted at the end of the optimization. It can be observed that carbons have

TABLE V. Binding energy and pore size diameter (PSD) where PSDW means whole system and PSD_R means the biggest ring in Fig. 8. Energy in [Kcal/mol], and pore size diameter in [Å].

Fig. 8	Ebinding	PSD_W	PSD_R
			2.84
a	-471.272		3.26
b	-501.731		3.35
c	-1609.841	4.53	3.53
d	-2328.804	5.8	5.8
e	-2996.576	7.4	7.4
f	-3196.626	7.3	4.1
g	-3443.472	6.85	3.8
h	-3537.683	7.07	4.7
i	-1951.536	6.8	6.42*
j	-4024.754	$\sim$	$\sim$5.4
k	-7710.915	8.08	8.08

*This case corresponds to psdsl

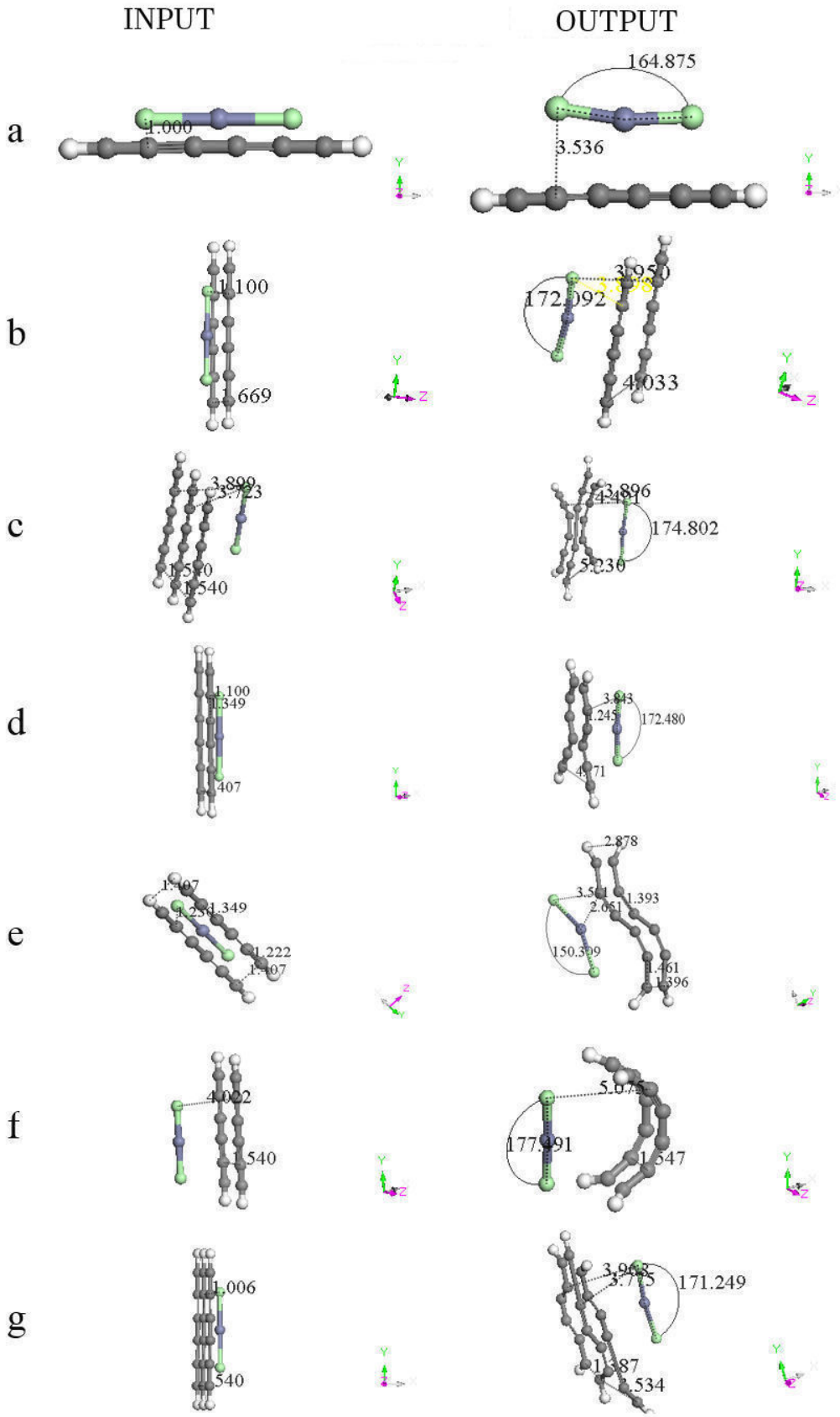

FIGURE 6. Input - Output scheme of the optimization energy corresponding to zinc salt which is near to one, two or three six carbon chains. The latter is forming new non-planar molecular structure in most of the cases. See Table III.

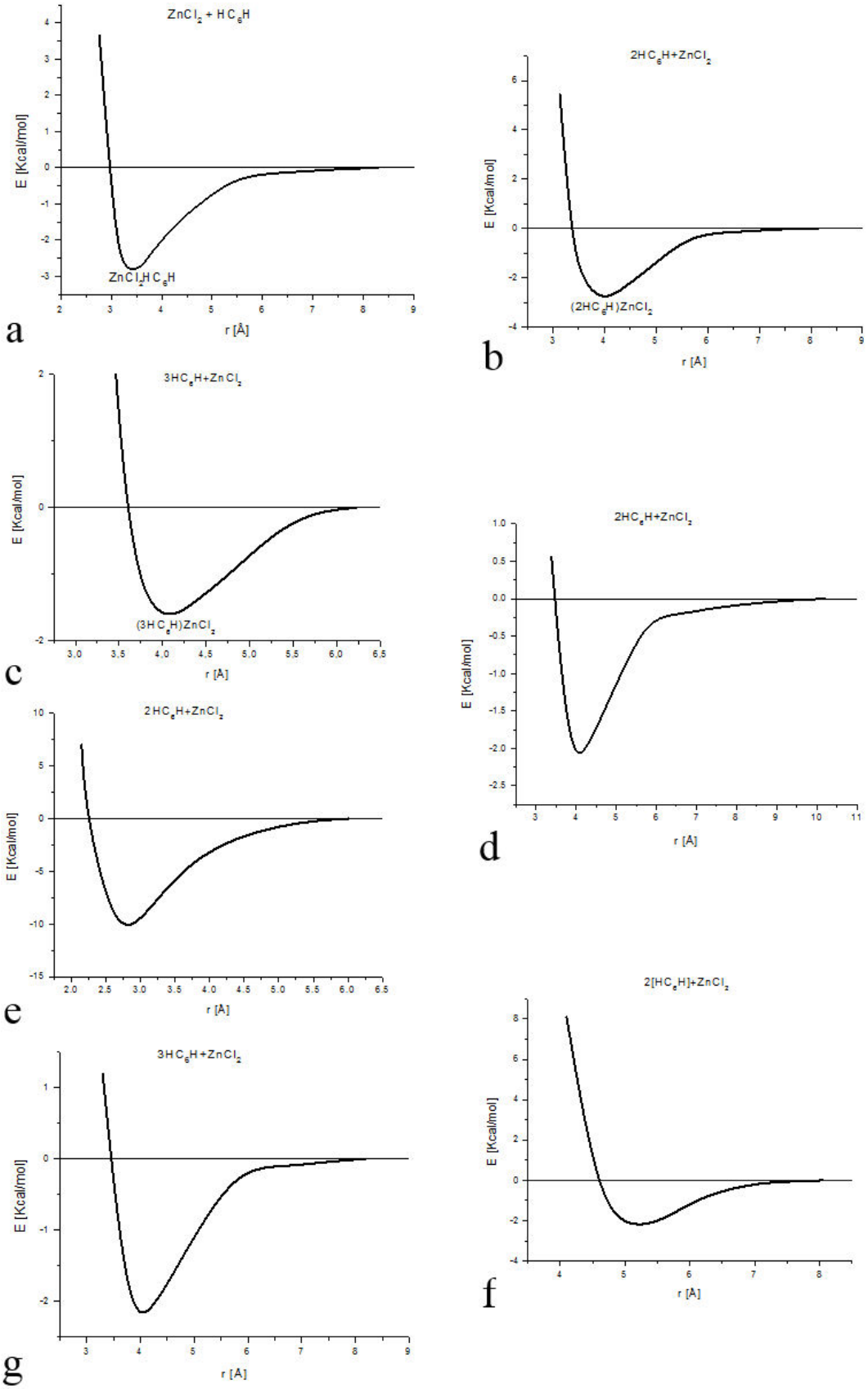

FIGURE 7. The potential energy curves corresponding to the output of Fig 6. The corresponding equilibrium distance and the equilibrium energy are given in Table IV. The size of the well depth or bond strength corresponds to the absolute value of the equilibrium energy.

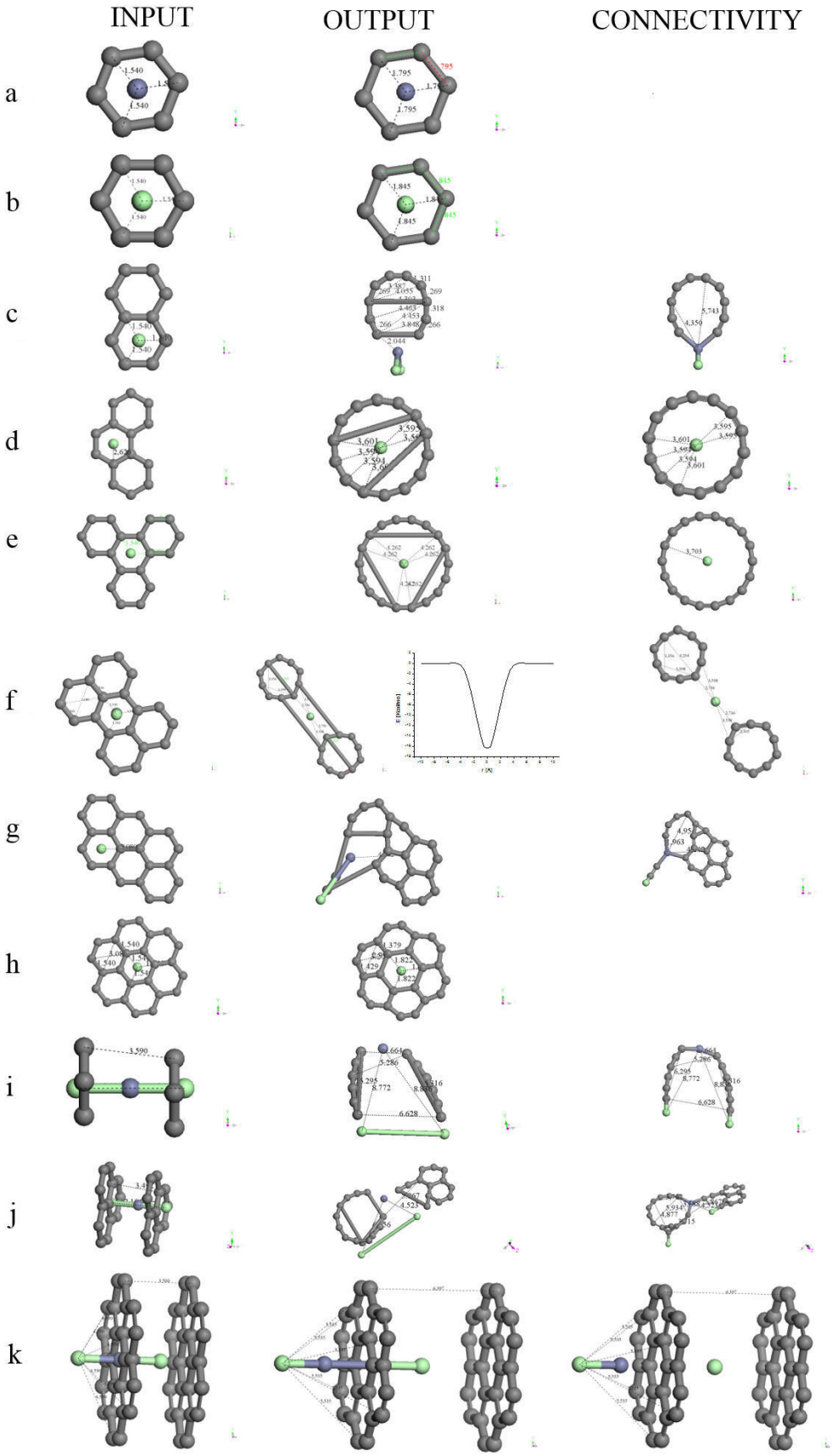

FIGURE 8. Input - Output scheme of geometry optimization corresponding to zinc salt acting on a specific hexagonal carbon ring as observed. See also Table V.

a tendency to form a circle due to the position in which the zinc salt is located at the beginning. Actually the area grew 31.2% because $A_O = 1.312A_I$ for $A_I = 12.3232 Å^2$, which is lower than the previous one. Connectivity calculation [24] exhibits clearly the insertion of zinc dichloride into a new carbon ring.

A new input is to add another hexagonal carbon ring as in Fig. 8d, then after the geometry optimization a polygonal carbon ring of 14 sides is observed. This confirms a tendency of carbon atoms to form circle rings. Furthermore, the area calculated using Heron formula is 25.56 $Å^2$. Using this as a circle area (πr^2), the pore size diameter can be approximated as $D = 2(A/\pi)^{1/2} = 5.8$ Å. Actually the diameter measured is 5.77 Å. In this case $A_O = 1.3827A_I$, where $A_I = 18.4848$ $Å^2$. Connectivity keep invariant these calculations, and the new molecule corresponds to one carbyne case [30].

A symmetrical addition of another hexagonal carbon ring in the input as in Fig. 8e provides a polygon of 18 sides after the geometry optimization in the output of this Figure. This is the best circle carbon ring obtained here with three bonds inside of the same, as disk morphology. The triangle area is $A_T = 42.18389$ $Å^2$, while the circle area is $A_C = 43.00840$ $Å^2$. They are almost the same. Here $A_O = 1.71156A_I$ which means ∼71.15% of growth. In this case the growth of the ring with zinc salt inside is $A_O = 4.4281A_I$ for $A_O = 6.1616$ $Å^2$ with a pore size of 5.894 Å, while in the previous case it is $A_O = 3.0799A_I$. Connectivity [24] calculation provides an 18-carbon ring sharing single and triple bonds, which corresponds to one carbyne molecule [30].

Completing 5 hexagonal carbon rings as in the input of Fig. 8f, and after the geometry optimization two decagonal carbon rings were obtained in the output, with one bond in the middle of each one, and connected by two bonds, where $A_O = 1.3524A_I$ for $A_I = 30.81$ $Å^2$. It is clear in this case that linear zinc dichloride molecule remains as a salt molecule because it is not broken or separated. The potential energy curve has a minimum in (0 [Å], 16 Kcal/mol), obtained in the x direction and taking vertically this molecule. Then adsorption is located in the threshold among physisorption and chemisorption for a potential well depth around 16 Kcal/mol. Connectivity calculation exhibit two 10-carbon ring alternating single and triple bonds, separated equidistantly from linear zinc dichloride. Another form of amorphous activated carbon comes out when six hexagonal carbon rings were joined, as in the input shown in Fig. 8g. In this case the area calculated in the output is lightly compacted: $A_O = 0.999256348A_I$ for $A_I = 36.969585$ $Å^2$. Connectivity calculation leads us to observe zinc atom bonded to three carbon atoms, and two carbon atoms stayed inserted in the zinc dichloride bonds leaving dichloride molecule in the carbon atom at the end. This new carbon molecule contaminated by zinc and chlorine has single, double, and triple bonds.

The last case here exhibited is when 7 hexagonal carbon rings were joined as in the input shown in Fig. 8h. After the geometry optimization the area in the output suffered a greater compression than in the previous case: $A_O = 0.909908362A_I$ for $A_I = 43.1312$ $Å^2$. The growing and compressing of the area after the geometry optimization is a clear indication of the existence of very different kind of pore size distribution in the amorphous activated carbon.

In case of stacking sheets of carbon rings, the initial point corresponds to 12 carbon atoms of two hexagonal carbon

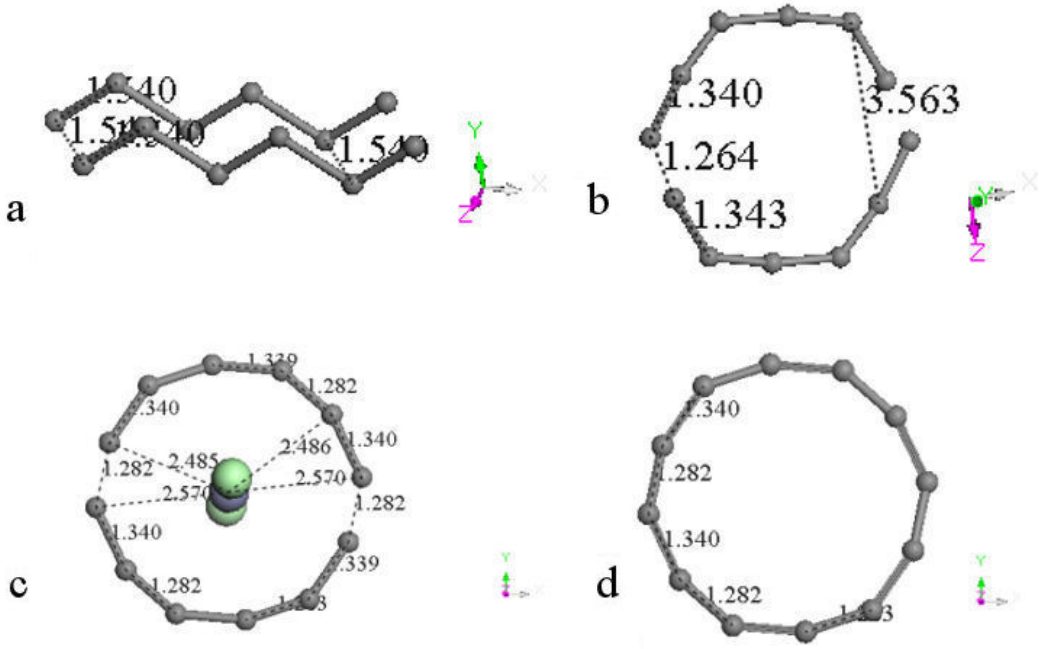

FIGURE 9. a) Two six carbon chains separated to a bond distance. b) These carbon chains change to a twelve carbon ring after geometry opyimization. c) Pore size area increase 4% after carbon activation with zinc salt. d) Connectivity of the activated carbon ring.

rings in face to face orientation, where zinc salt is perpendicularly located among both rings as observed in Fig. 8i, and from the geometry optimization shown in the output A = 32.448 Å^2 is calculated. Then 6.4276 Å^2 is the pore size diameter approximately, which for a small system like this, with just one zinc salt molecule and 2 hexagonal carbon rings is a good result. After connectivity calculation chlorine atoms stayed bond to the lowest carbon atoms, while zinc is bonded to the highest carbon atoms in Fig 8i.

One stacking of two sheets case is exhibited in Fig. 8j. These are 26 carbon atoms showing the particular amorphous activated carbon form after geometry optimization of a dimmer of two sheets of three carbon rings in face to face orientation. The area of the biggest ring after optimization is ∼15 Å^2 which corresponds to ∼4.37 Å of pore size diameter approximately. Then the area of this ring grew ∼2.43 times. Connectivity calculation lead to ∼5.4 Å of pore size diameter of the biggest ring, and to a carbon molecule contaminated by zinc, and also by chlorine in different places, because zinc share three carbon atoms while chlorine share only one carbon atom as if this were a hydrogen atom.

Another stacking of two sheets is exhibited in Fig. 8k. These are 48 carbon atoms showing activated carbon after geometry optimization of a dimmer of two sheets of seven carbon rings in face to face orientation. The input volume among graphitic carbon sheets is 150.959 Å^3, and after optimization is 275.91 Å^3 which corresponds to 8.08 Å of pore size diameter. Then the volume grew 82.8 % or $A_O = 1.8277A_I$. Connectivity calculation lead to separation of zinc salt molecule as ZnCl+Cl, and while the chlorine atom stayed between the two graphitic carbon sheets, the ZnCl molecule keeps far away from the closest graphitic sheet.

These two cases have in common the metal separation bond of the chlorine atoms, showing that carbon is a natural adsorbent of metals, and sending the chlorine atoms until the end. These two geometry optimizations, first of a dimmer of just one hexagonal carbon ring in face to face orientation with one zinc salt molecule, and second of a dimmer of hexagonal carbons also in face to face orientation, with zinc salt crossing each sheet of three hexagonal carbon rings, were able to separate the bonds of zinc dichloride in a complex $[2C_{13}]ZnCl_2 \rightarrow ClC_{13}ZnC_{13}Cl$ and a complex $[2C_6]ZnCl_2 \rightarrow ClC_6ZnC_6Cl$. While the first complex is non-planar, the second one is planar.

3.7. Diamond-like carbon plus $ZnCl_2$ interaction

For activating diamond using zinc dichloride as activating agent, through a Geometry optimization, DMol^3 mGGA/M06-L functional is applied in order to build an optimized diamond-like structure, in the following steps. First the geometry of a C_6 ring is optimized. Second, to the latter we added the missing four carbons for optimizing the whole sp^2 structure of a unit diamond. Third, the whole unit structure diamond of fourteen carbons is optimized. Finally an optimized zinc dichloride molecule is placed as observed in Fig. 10a,b as input-output of the geometry optimization searched. A potential energy curve when the activating agent cross this diamond-like molecule in x-direction as shown in Fig. 10c. A potential well depth around 20 Kcal/mol means chemisorption when zinc dichloride is inside the diamond-like molecule. When this activating agent is going out the maximum around 5 Å means a very strong chemisorption, and the minimum around 13 Å corresponds to a physisorption.

Applying an average calculation to the input-output bond lengths of diamond-like molecule, ∼18% growing of activated carbon of diamond with zinc-dichloride is observed. Diamond formula is $C_{14}H_{24}$, with density 3.514 gr/cm^3 [31], and mass 192.34 gr, then diamond volume is 54.74 cm^3, and activated diamond volume is 64.59 cm^3. Graphite density is 2.266 gr/cm^3 [31], with sp^2 hybridization, then

$$\rho_{ad} = 1.3141\rho_g, \quad \text{and} \quad \rho_{ad} = 0.847\rho_d$$

where ρ_{ad} is density of activated diamond, ρ_g is graphite density and ρ_d is diamond density. Therefore

$$\rho_g < \rho_{ad} < \rho_d$$

in diamond there is sp^3 hybridization of four carbons, sp^2 of six carbons, and the last four carbon share all its free electrons. This means that 40% is sp^3, and 60% is sp^2.

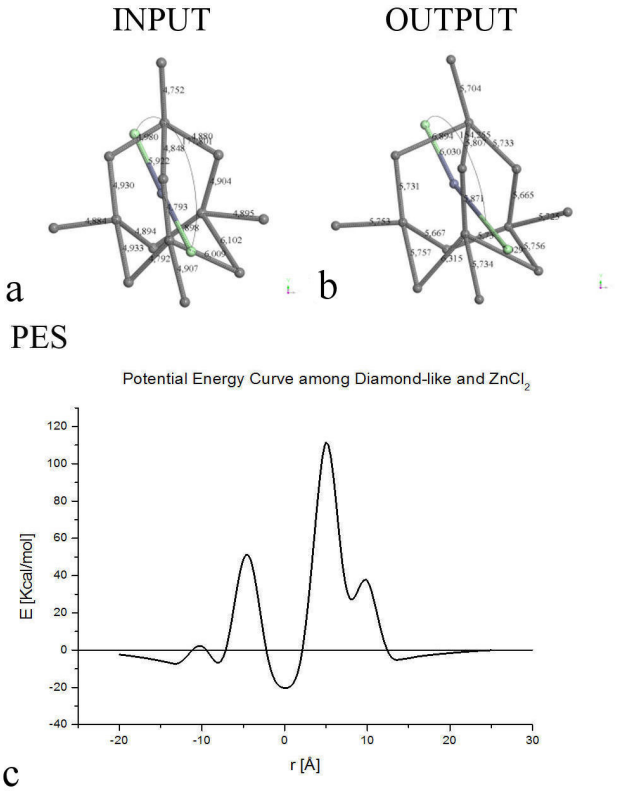

FIGURE 10. a) Input: Optimized diamond molecule. b) Output: Activated carbons of a diamond. c) Potential energy curve of the interaction Diamond + Zinc Dichloride.

4. Discussion

Our different geometry optimizations obtained for very similar cases take us to consider that PSD may appear in: i) inside carbon rings that we define as psdcr, ii) between graphitic sheet layers forming cavities that we define as psdsl, and iii) inside granular diamond-like carbon that we define as psdgd. In the psdcr case there are two results 3.8 Å and 7.4 Å of pore size diameter for those shown in Figs. 4c and 8e, respectively. In case of psdsl Fig. 8k provides the best 8.08 Å pore size diameter, very close to the most populated pore size distribution 9.0 Å diameter. In case of psdgd our system grew 18% only, with 4.98 Å of pore size diameter. Our best calculation of pore size diameter for one carbon ring is 8.02 Å, which is around the order of 55% of those experimentally measured for activating carbon using $ZnCl_2$. We applied connectivity [24] calculations in many cases of Fig. 8, due to unrealistic long bonds, and considering that connectivity and PSE methods produce similar results in chemisorption cases, and SCF calculations do not converge to build potential energy curves in most of these cases. Connectivity of ionic or covalent bonds allow to observe active carbon with zinc chemically adsorbed in Figs. 8c, 8h-8j. Then the orientation of the interaction can provide a big percentage of zinc inserted in activated carbon when using zinc dichloride as activating agent. Scattering data take us to average potential energy curves [32,33] hiding information about physisorption or chemisorption, because the orientation of the interaction is not important when taking this kind of data.

The use of six-carbon chains in this model is due to graphite and graphene are hexagonal carbon sheets. One very good example is shown in Fig. 9, where two linear six-carbon chains after geometry optimization form one ring of twelve carbons with an Area of 18.39 $Å^2$ and pore size diameter 4.84 Å (Fig. 9b). Activating this carbon ring with zinc dichloride provides a pore size diameter of 4.94 Å (Fig. 9c) with only 4.2% of growth, and close to the largest values obtained previously. We also see in Fig. 9d that calculating connectivity single and triple bonds appear, consequently this twelve carbon ring is strongly bonded with σ and π electronic configuration interactions.

Considering that $ZnCl_2$ push carbon, we also propose that the equilibrium distance Re in Tables I and IV allows pore size diameters among 5.3 Å and 10.4 Å close to those measured previously. Our results have a close agreement with experimental micropore size distributions (MPSD) measurements of activated carbon around 9 Å and agree with the lowest values of average micropore width. We must note that Fig. 8e exhibits a disk form after geometry optimization. Due to this fact, it is easy to imagine more regular geometries as cylinders and spheres also formed when carbon is under the action of metal activating agents. In crude oil fields nickel is a natural activating agent of carbon molecules, and disks, cylinders or spheres have been widely detected [34].

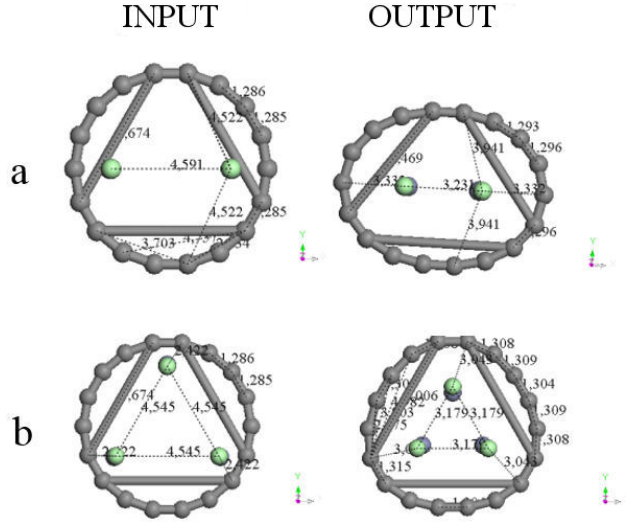

FIGURE 11. Input-Output of adding more zinc salt to the system obtained in Fig. 8e.

We applied two and three zinc salt molecules inside the 18-side carbon ring obtained after geometry optimization, and we applied geometry optimization again. Figure 11 exhibit these two cases. In the former case we only observe deformation as an ellipse of the 18-carbon molecule, because the area stays invariant. In the latter case we observe a small growing of the area, because the pore size diameter grew from 7.4 to 7.52 Å.

Zinc dichloride is a salt that can be washed from the activated carbon when the $[2C_6]ZnCl_2$ molecules are in contact with water, however zinc has been detected in activated carbon after its cleaning.

5. Conclusions

First, the tendency of linear chains after geometry optimization is to form aromatic rings; however, we used two linear carbon chains which after optimization changed to amorphous carbon. The latter occurs when they get in contact with zinc dichloride under the action of a geometry optimization. Second, there is a very strong potential well depth 175 kcal/mol among the twelve carbons and zinc dichloride, which is indicative of a chemisorption according to the range handled by Atkins [29]; however, in polyyne carbon case all the potential well depths are lower than 11 kcal/mol corresponding to physisorption. This means that even a small quantity of hydrogen, adsorption changes significantly. Activated carbon morphology depends on the carbon and on the methodology used.

Our best model provided a pore size diameter of 8.08 Å in agreement to experimental results for the average pore size distribution diameter. Improvements are still in development considering carbon chains (linear or rings) greater than six-carbon molecules, and more molecules of zinc salt or another activating agent. Linear Carbon interactions tend to form carbon rings after geometry optimization, and accord-

ing to the case they stay either linear or planar or non-planar. We consider planar as graphitizing and non-planar as non-graphitizing AC.

A true formation of $[2C_6]ZnCl_2$ molecules are obtained at the potential well when one molecule of two six-carbon chains interacts with $ZnCl_2$, which have to be washed in order to improve quality of activated carbon. Our results give evidence that at particular cases Fig. 8g, i, j, carbon stayed inserted in the bonds of $ZnCl_2$ molecule, then zinc might appear in the composition of activated carbon using zinc dichloride as activating agent, despite washing.

Acknowledgments

This work was supported by DGEST under grant 5164.13-P; and it was developed under a project with ITESM. Thanks for their facilities.

1. J. Jagiello, A. Ansón, and M.T. Martínez, *J. Phys. Chem. B* **110** (2006) 4531.
2. H. Tanahashi, *J. Appl. Electrochem.* **35** (2005) 1067.
3. L.A. García *et al*., *presented at the 14th International Symposium on Metastable and Nano Materials*, Corfu, Greece, 2007.
4. A. Allwar, Bin Md Noor and A. Bin Mohd Nawi, *Journal of Physical Science* **19** (2008) 93.
5. D. Lozano-Castelló, D. Cazorla-Amorós, and A. Linares-Solano, *Energy & Fuels* **16** (2002) 1321.
6. P.A. Gauden, A.P. Terzyk, G. Rychlicki, P. Kowalczyk, M.S. Ćwiertnia, and J.K. Garbacz, *J. Coll. Int. Sci*. **273** (2004) 39.
7. R.Ch. Bansal, and M. Goyal, *Activated Carbon Adsorption*, *CRC Press* (Taylor & Francis, Florida, 2005).
8. F. Çeçen and Ö Aktaş, *Activated Carbon for Water and Wastewater Treatment Integration of Adsorption and Biological Treatment*, (Wiley-VCH, Weinheim, Germany, 2012).
9. R.E. Franklin, *Proc. R. Soc. A*, **209** (1951) 196.
10. P.J.F. Harris, Liu Zheng and Suenaga Kazu, *J. Phys.: Condens. Matter* **20** (2008) 362201.
11. T. Iyama, H. Kawabata, and H. Tachikawa, *Jpn. J. Appl. Phys.* **47** (2008) 803.
12. Y. Hu, T. Wu, W. Liu, L. Zhang, and R. Pan, *J. Phys. Chem. A* **118** (2014) 1918.
13. C. Ricolleau, Y. Le Bouar, H. Amara, O. Landon-Cardinal, and D. Alloyeau, *J. Appl. Phys.* **114** (2013) 213504.
14. S. Cerny, Active carbon manufacture, properties and applications, (Elsevier Publ. Co., Amsterdam, 1970).
15. K. Berman and B. Katz, US Patent No. WO20000429 A120000106 (1998)
16. B. Baker, US patent No. 5,965,483 (12 October 1999).
17. IUPAC commission on Colloid and Surface Chemistry Including Catalysis, *Pure Appl. Chem.* **57** (1985) 603.
18. Y. Zhikuan, E.D. Tolles, J.C. McCue and Zhiquan Q. Ya, Westvaco Corp. US Patent No. 5,538,932 (23 July 1996).
19. T. Kazuo, US Patent No. 5,994,261 (30 November 1999).
20. L. Zhou, Y. Zhou and Y. Sun, *International Journal of Hydrogen Energy* **29** (2004) 475.
21. B. Delley, *J. Chem. Phys.* **92** (1990) 508; B. Delley, *J. Chem. Phys.* **113** (2000) 7756.
22. J.P. Perdew, Y. Wang, *Phys. Rev. B* **45** (1992) 13244.
23. J.P. Perdew, Y. Wang, *Phys. Rev. B*. **33** (1986) 8800.
24. K.P. Huber and G. Herzberg, *Molecular Spectra and Molecular Structure* **IV** constants of diatomic molecules, (Van Nostrand Reinhold Company, 1979).
25. A.D. Becke, *J. Chem. Phys.* **88** (1988) 1053.
26. R.H. Baughmann, *Science* **312** (2006) 1009.
27. H. Ding, T.W. Schmidt, T. Pino, F. Güthe, J.P. Maier, *Phys. Chem. Chem. Phys.* **5** (2003) 4772.
28. P.W. Atkins, *Physical Chemistry*, (Oxford University Press, NY 2001); A.M. Blas, *Bs Thesis*, ESIQIE Instituto Politécnico Nacional, México, 1981.
29. E. Estrada, *J. Phys. Chem. A* **106** (2002) 9085.
30. M. Liu, V.I. Artyukhov, H. Lee, F. Xu, and B. I. Yakobson, *ACS Nano* **7** (2013) 10075-10082.
31. N.N. Greengood and A. Earnshaw, *Chemistry of Elements*, Butterworth/Heinemann Second Edition Oxford UK 1997.
32. F. Álvarez-Ramírez, E. Ramírez-Jaramillo, Y. Ruiz-Morales, *Energy & Fuels* **20** (2006) 195.
33. E. Gasca, J.H. Pacheco, F. Álvarez, IJCNN (International Joint Conference on Neural Networks) IEEE-INNS-ENNS, (2009) 946.
34. J.H. Pacheco-Sánchez, G.A. Mansoori, *Rev. Mex. Fis.* **59** (2013) 584.